Materials Science Forum Vols. 102 - 104 (1992) pp. 85-98

HARDNESS, MELTING REACTIONS AND HEAT TREATMENT OF Al-Si-Cu-Mg ALLOYS REINFORCED WITH ALUMINIUMOXIDE PARTICLES

M.J. Starink, V. Jooris and P. van Mourik

Laboratory of Metallurgy, Delft University of Technology, Rotterdamseweg 137, NL-2628 AL Delft, The Netherlands

ABSTRACT

Results of a study mainly by Differential Scanning Calorimetry (DSC) on an Al-20at%Si-1.5at%Cu-1at%Mg (ASCM) alloy with 0, 2.5, 5, and 10 vol% aluminiumoxide (Al_2O_3) particles are reported. The alloys were produced by gas atomisation, mixing with particles and subsequent extrusion. DSC scans of the as-extruded alloys showed no precipitation reactions. Between 780 and 800 K the melting of the Q ($Al_5Cu_2Mg_8Si_6$) and the Al_7Cu_2Fe (ASCM contains a small amount of iron) phases was observed. On heating the matrix melts between about 810 K to 840 K, subsequently silicon dissolves in the melt. The microstructure of the AE alloys with Al_2O_3 particles (size about 1 to 6 μm) showed no clustering of Al_2O_3 particles. During DSC after solid quenching the formation of GPB zones was observed. After dissolution of the zones, Q phase and θ phase precipitate. Hardness measurements show, that both GPB zones and Q phase precipitates can improve the room-temperature strength of the ASCM alloy by about 75%, compared to the as-extruded alloy. Heat treatments producing GP or GPB zones (ageing at temperatures below about 440 K) do not contribute to the strength of the alloy at elevated temperature. Q-phase precipitates improve the hardness after an additional overageing treatment at 473 K by about 60% (as compared to the as-extruded alloy).

1. INTRODUCTION

The wear resistance of aluminum alloys can be improved by the introduction of finely dispersed hard particles to the alloy [1,2]. For example, a fine dispersion of silicon particles can be obtained by rapid solidification of a molten aluminum alloy with a high silicon content [3]. A dispersion of ceramic particles in aluminium alloys can be obtained via various production routes, e.g. by compocasting or by mixing particles with aluminium alloy powders followed by extrusion. Metals reinforced by dispersed (ceramic) particles are generally referred to as Metal Matrix Composites (MMCs). Their increased wear resistance, low thermal expansion and improved high-temperature strength, make MMCs attractive for applications like parts of combustion engines.

In this contribution, results of a study on the heat treatment of Al-20at%Si-1.5at%Cu-1.1at%Mg (ASCM) alloys reinforced with 0, 2.5, 5, and 10 vol% aluminiumoxide (Al_2O_3) particles are presented. These alloys combine the presence of two reinforcing components (silicon and Al_2O_3 particles) with the possibility of age hardening of the Al-rich phase. Hence, an appropriate heat treatment is necessary to optimize the mechanical properties at room and elevated temperatures. The

presence of dispersed particles in solid-quenched age-hardenable aluminium alloys generally influences the kinetics and sequences of precipitation processes, as compared to corresponding unreinforced alloys [4]. Appropriate heat-treatment procedures for these alloys are, as yet, unknown. This applies for both the solution annealing treatment (temperature) and the age hardening (temperature and time). Therefore, it is necessary to establish appropriate solid-solution temperatures and age-hardening procedures for MMCs. Hence, melting and precipitation phenomena should be investigated. As melting and precipitation involve large enthalpy changes, differential scanning calorimetry (DSC) was used as the main investigation method. Besides, hardness measurements, optical microscopy and X-ray diffraction were applied as well.

2. EXPERIMENTAL PROCEDURES

2.1. PRODUCTION ROUTE

The alloys under investigation were made available the Japanese firm Showa Denko K.K. The base alloy was rapidly solidified by gas atomisation, yielding fine powder (sizes range from 1 to 100 μm, with a median size of about 24 μm [5]). The cooling rate during gas atomisation is generally about 10^4 to 10^6 K/s [3]. Subsequently, the powder was mixed with ceramic Al_2O_3 particles, in order to obtain mixtures with 0, 2.5, 5 and 10 volume percent of ceramic particles. Finally, the mixtures were extruded at about 670 K into round bars with a diameter of about 20 mm.

The chemical compositions of the extruded alloys are presented in Table 1. The four alloys are indicated by ASCM0, ASCM2.5, ASCM5 and ASCM10, in which the last number refers to the volume percentage Al_2O_3 particles. The main impurities in the base alloy (as measured by X-ray fluorescence) are: Ni (~0.02 at%), Zn (~0.01 at%), Ti(~0.006 at%) and Cr (~0.005 at%).

Table 1 : Composition of the alloys and the base alloys.

alloy name	Al_2O_3	Si		Cu		Mg		Fe	
		alloy	base	alloy	base	alloy	base	alloy	base
	vol % *)	wt%	at%	wt%	at%	wt%	at%	wt%	at%
ASCM0	-	20.2	19.9	3.47	1.52	0.96	1.10	0.24	0.12
ASCM2.5	2.5	19.7	20.2	3.44	1.56	0.89	1.05	0.24	0.12
ASCM5	5.2	18.9	20.1	3.32	1.57	0.88	1.09	0.23	0.12
ASCM10	10.4	16.9	19.6	2.97	1.52	0.77	1.03	0.20	0.11

*) Calculated from measured weight percentages using the densities of the ASCM base alloy, 2.67 g/cm^3 and of α-Al_2O_3, 3.98 g/cm^3 [6].

2.2. DIFFERENTIAL SCANNING CALORIMETRY

A DuPont 910 differential scanning calorimeter was used. Inside the DSC cell a protective gas atmosphere was maintained by flushing with 99.999% pure argon (flushing started 10 min before the experiment). Both specimen and reference were enclosed in an aluminium pan with an aluminium cover. Heating rates between 0.5 and 40 K/min were used. Per specimen three scans were performed; the second after cooling at about 10 K/min and the third after cooling at 2 K/min. The calibration procedures and baseline corrections were described earlier [7].

2.3. HEAT TREATMENT

Experiments were performed on specimens after various production stages and heat treatments. These are denoted as follows :

- LQ: liquid-quenched, gas-atomised powder (stored at room temperature).
- AE: as-extruded alloy (stored at room temperature).

- SQ: solution-annealed (10 min at 768 K) and quenched (in water at room temperature) AE specimen. The SQ specimens were stored at room temperature for 1 hour after quenching.
- SQ NA(x h): an SQ specimen aged at room temperature for x hours.
- SQ DSC(y K): an SQ specimen heated to y K inside the DSC cell at a heating rate 2 K/min, and subsequently cooled down to room temperature at about 10 K/min. This cooling rate is sufficiently fast (as compared to the heating rate) to avoid reactions during cooling.
- SQ AA(z K): an SQ specimen aged at room temperature for 4 days, and subsequently artificially aged at z K for 24 hours.

To investigate mechanical properties after a long-time application at elevated temperatures, hardness measurements were performed on selected specimens which were aged at 473 K for four days (esentially an additional overageing treatment, see section 3.3). All artificial ageing treatments were performed in an oil bath with temperature control within 1.5 K.

2.4. OPTICAL MICROSCOPY AND HARDNESS MEASUREMENTS

Vickers hardness (Hv) was measured on polished surfaces parallel to the extrusion direction. The apparatus used was a Leitz-Durimet hardness tester with an indentation force of 981 N. The values reported are the average of ten determinations; the given errors equal the standard deviation.

Jena Neophot 30 and Jena Neophot 2 optical microscopes were used to characterize the microstructures and the distribution of Al_2O_3 particles. Polished specimens were etched with a 1:1 mixture of Keller and Wilcox reagent and 5% Nital.

2.5. X-RAY DIFFRACTION

For identification of phases, X-ray diffraction was performed using a Guinier camera. Diffraction patterns of the AE ASCM0 alloy at room temperature and of SQ ASCM0 during heating at a constant rate (0.5 K/min) from 293 to 773 K were recorded.

3. RESULTS

3.1. GAS-ATOMISED POWDERS

DSC scans of the gas-atomised ASCM powder are presented in Fig. 1. During the first scan the heat flow is exothermic over almost the entire temperature range, except for a small endothermic effect in the temperature range 360 to 420 K. After this endothermic effect a clearly defined exothermic effect is observed, with peak temperature 480 K. Since this effect seems to overlap with an exothermic effect located around 570 K, the end temperature of the effect around 480 K is not clearly identifiable. The heat content of the effect around 480 K, ΔQ_{MP} , is estimated by integration of the heat flow from 420 to 535 K. The value thus found is 607 J/mole ASCM powder. Beyond 590 K the heat flow continues to be exothermic. The heat flow in this temperature range does not show a clearly defined peak. In the second and the third runs no exothermic effects are observed. Instead, both runs show an endothermic effect beyond 550 K.

After completion of the three runs the mass of the powder specimen was higher than at the start of the experiment. The increase amounted to 39±5 µg, which corresponds to 0.17% of the original mass of the specimen.

3.2. AS-EXTRUDED ALLOYS

Isothermal X-ray diffraction (at 298 K) reveals the presence of the following phases in the AE ASCM0 alloy: the Al-rich phase, the Si phase (diamond structure), the θ phase (Al_2Cu), the Q phase ($Al_5Cu_2Mg_8Si_6$) and the Al_7Cu_2Fe phase.

In Figs. 2a to c optical micrographs of AE ASCM, ASCM5 and ASCM10 are presented. The following observations are made:

i. Although bands along the extrusion direction seem to be enriched with Al_2O_3 particles (black colour), no clustering of Al_2O_3 particles is observed.
ii. The sizes of the irregular shaped Al_2O_3 particles range from about 1 to 6 μm, with an average of about 2 μm.
iii. Elongated Al_2O_3 particles are aligned along the extrusion direction.
iv. The Si-phase particles (dark grey), which are homogeneously dispersed in the Al-rich phase (light grey), have a grain size between about 1 and 10 μm, with an average of about 4 μm.
v. Also a third type of precipitate (grey) can locally be discerned. Considering the phase identification by X-ray diffraction, these are probably Q or Al_7Cu_2Fe-phase precipitates.

By increasing the etching time to about 1 min, the grain boudaries of the Al-rich phase become visible (pictures not presented here). The grain size of the Al-rich phase is about 5 μm.

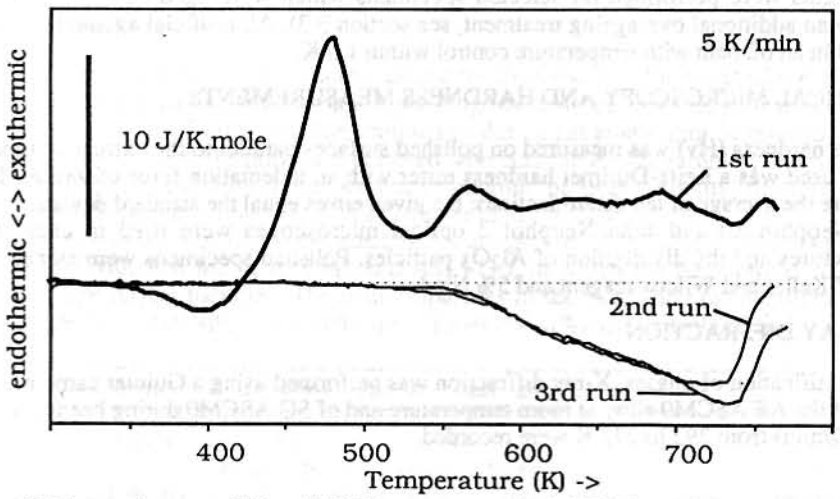

Fig. 1: DSC scans between 293 and 773 K on gas-atomized ASCM powder.

2a

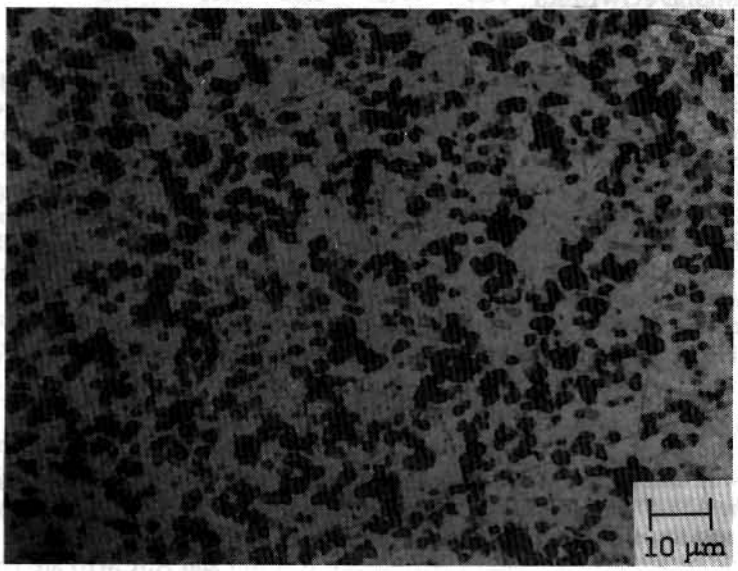

2b

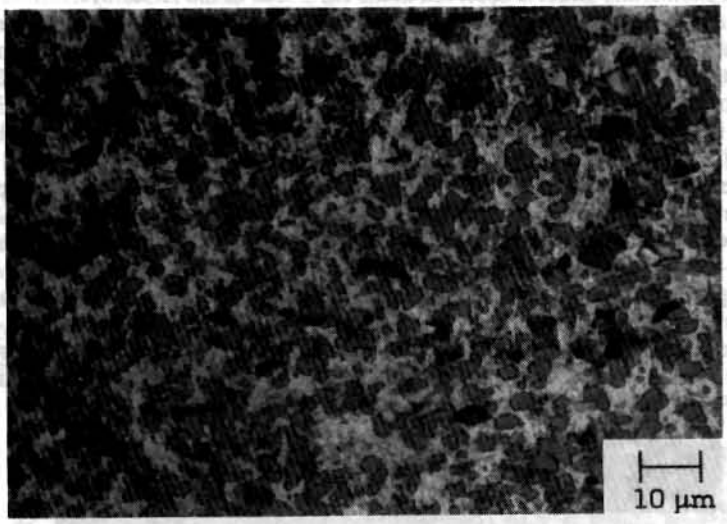

2c

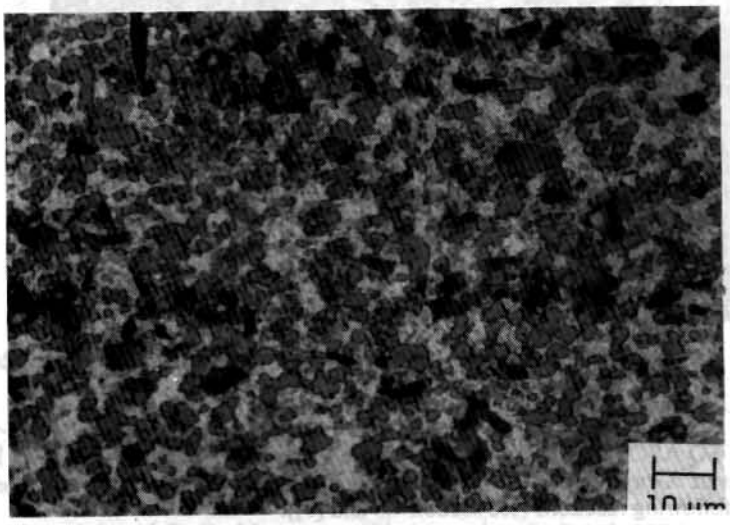

Fig. 2a to c : Optical micrographs of longitudinal sections of AE ASCM0, ASCM5 and ASCM10. Extrusion direction is horizontal. Etching time: 10 sec.

In Fig. 3, taken from an AE ASCM0 specimen heated twice to 890 K, severe coarsening of silicon particles and clustering of the Al_2O_3 particles is observed.

DSC experiments were performed on AE ASCM0 and AE ASCM10. These experiments were aimed at determining a suitable temperature for solution annealing before solid quenching. During solution annealing, melting should be avoided and hence the temperature at which melting starts has to be known. Fig. 4 shows the first and the second DSC runs on AE ASCM0. For a temperature range of 750 to 860 K, Fig. 5 shows the second and the third DSC runs on AE ASCM10, which were performed after a first DSC run until 773 K. Note that in Fig. 5 only endothermic effects are observed, and that the effects are much larger than the ones shown in Fig. 4. The effects shown in Fig. 5 are caused by melting reactions, while those in Fig. 4 are caused by dissolution reactions (see section 4.2). The following observations are made:

i. No substantial exothermic effect is observed in the DSC scan of the AE alloys.
ii. Both the first and the second run of AE ASCM0 (Fig. 4) are dominated by an endothermic effect, which starts at 610 K. This endothermic effect seems to be divided into at least two subeffects: one effect continues upto about 750 K, while the other effect continues beyond 785 K.
iii. The melting of the SQ ASCM10 alloy is subdivided into several seperate stages. Four melting reactions are indicated by A, B, C, and D (see Fig. 5). Effect C is by far the largest. Effect D seems to continue beyond the temperature range studied in this experiment.

Comparison of the DSC runs presented in Figs. 4 and 5 with DSC runs of AE ASCM10 performed at heating rate 20 K/min (not presented here) additionally shows:

iv. The end temperature of the first endothermic subeffect in Fig. 4 is largely uninfluenced by heating rate or Al_2O_3-particle content.
v. The peak temperatures of the melting reactions are independent of reactions heating rate or Al_2O_3-particle content.

For the temperature of solution annealing before solid quenching, a temperature below the start of melting should be selected. In order to have a safety margin of about 10 K to the start of melting we have chosen 768 K as solution annealing temperature (see section 4.2).

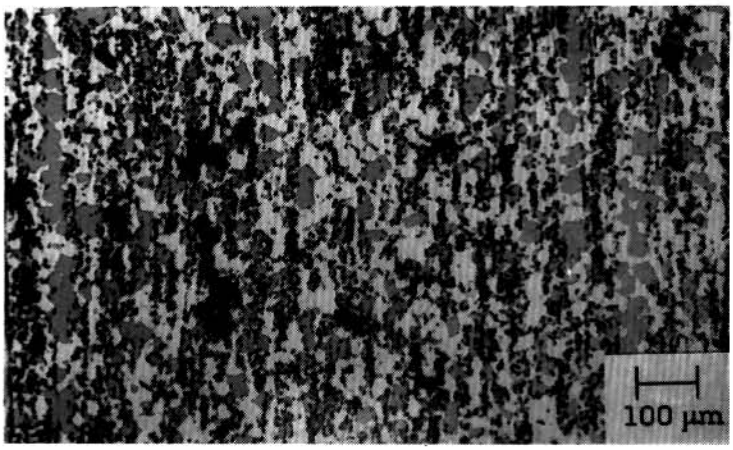

Fig. 3 : Optical micrograph of AE ASCM10 heated twice to 890K. Etching time 10 sec.

3.3. SOLID-QUENCHED AND HEAT-TREATED ALLOYS

DSC scans of SQ ASCM0 and ASCM10 alloys are presented in Fig. 6. In line with literature data and on the basis of X-ray diffraction, the effects occurring in the DSC of scans these alloys are attributed to the following reactions (see section 4.3 and [7]):

i. the formation of GPB (Al-Cu-Mg) zones,
ii. the dissolution of GPB zones,
iii. precipitation of the Q phase ($Al_5Cu_2Mg_8Si_6$),
iv. precipitation of the θ' and θ phases (both Al_2Cu),
v. the dissolution of the Q and θ phases.

Only effect i can be considered as a separated effect, the other effects show overlap. The influence of the presence of Al_2O_3 particles on the DSC curves of the SQ alloys is rather small. For a discussion of the influence of Al_2O_3 particles on the precipitation kinetics in SQ ASCM alloys, see Ref. 7.

The room-temperature hardness of SQ ASCM0 was measured after various heat treatments (see section 2.3). The results are gathered in Figs. 7 and 8. In Fig. 7 the room-temperature hardness of SQ DSC specimens are plotted as a function of DSC end temperature, together with the room-temperature hardness of the same specimens after an additional overageing treatment (4 days at 473 K). In Fig. 8, the room-temperature hardness of SQ ASCM0 after various heat treatments is compared with the

room-temperature hardness of the same specimens after the additional overageing treatment. The following observations are made.

i. The maximum hardness, both after initial heat treatment and after the additional overageing treatment, is obtained for the SQ DSC(487 K) specimen. This DSC end temperature corresponds to the end temperature of effect iii observed during the DSC scan.
ii. Natural ageing of SQ ASCM0 results in a remarkable increase of hardness.
iii. Artificial ageing of SQ ASCM0 for 24 hours at 393 K and at 433 K also yields a remarkable hardness increase.
iv. The additional overageing treatment considerably decreases the hardness the specimens (with the exception of the SQ DSC(575 K) specimen), but even then, the hardness of the heat treated specimens remains higher than that of the AE ASCM0 specimen.
v. After the additional overageing treatment the hardness of nearly all solid-quenched and subsequently aged specimens has dropped to about 120 HV. The only exceptions are SQ DSC(487 K) and SQ DSC (507 K) which retain a hardness of about 140 HV after additional overageing.

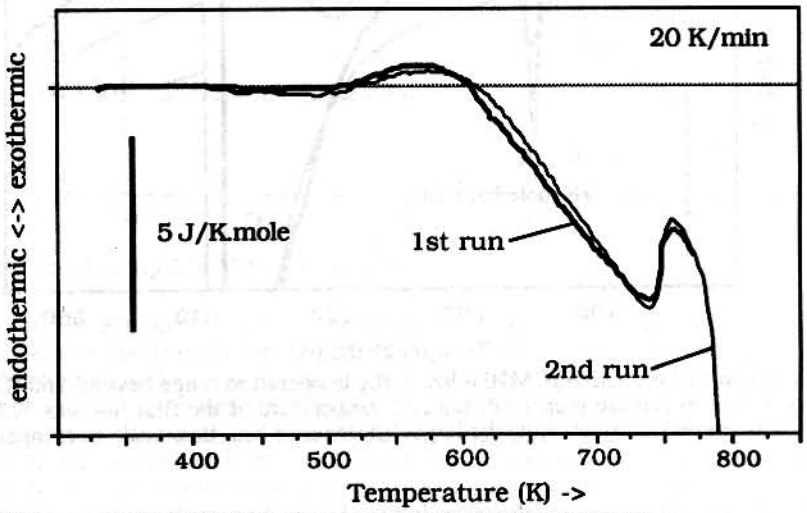

Fig. 4 : DSC scans of AE ASCM0 in the temperature range below 790 K.

4. DISCUSSION

4.1. GAS-ATOMISED POWDERS

The liquidus of the Al-Si-Cu-Mg system [8] shows that during slow cooling of the molten Al-20at%Si-1.5at%Cu-1.1at%Mg (the small amount of Fe will be neglected in this part of the discussion) the solidification starts with the following reactions:

liq -> Si (1)
liq -> Si + Mg_2Si (2)

During the completion of the solidification, the initially formed Mg_2Si will disappear again (Mg_2Si is not stable below about 790 K [8]), and the Q phase will form. This proceeds via the reaction [8]:

liq + Mg_2Si + Si -> Q + Al (3)

This peritectic reaction occurs at 802 K [8]. Since above this temperature no copper containing phases are formed, it is assumed that above 802 K the solidification process can be described on the basis of the Al-Mg-Si phase diagram. From this diagram [8] follows that during cooling the Al-rich phase will start to form at 828 K with the following reaction:

liq -> Al+Si+Mg_2Si (4)

During gas atomisation, the solidification rate is very fast : about 10^5 K/sec [3]. For the peritectic reaction 3, relatively slow solid state diffusion is necessary. It is thus expected that during rapid solidification the peritectic reaction 3 is suppressed, leading to the presence of metastable Mg_2Si in the rapidly solidified powder, as was observed by Estrada and Duszczyk [3].

Rapid quenching from the melt directly to room temperature, e.g. gas atomisation, can generally result in a supersaturated Al-rich phase. The amount of Si dissolved in the Al-rich phase of rapidly solidified hyper eutectic Al-Si alloys can be as high as 3.3at%, which is much larger than the maximum equilibrium solid solubility [9]. Hence, a high atomic fraction of Si dissolved in the Al-rich phase of the in the gas-atomised ASCM alloys is expected.

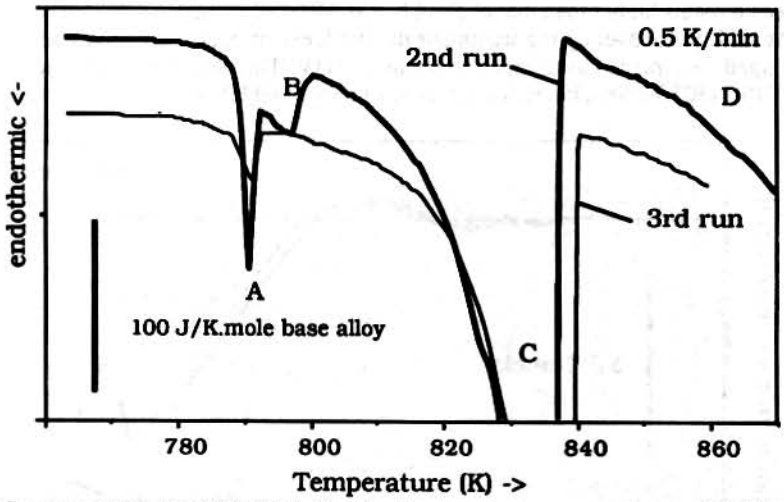

Fig. 5 : DSC scans of the AE ASCM10 alloy in the temperature range beyond 760 K. The second and the third run are presented; the end temperature of the first run was 773 K. All heat effects are endothermic. Note the large difference in heat flow scale as compared to Figs. 4 and 6.

For hypoeutectic, binary Al-rich alloys, including Al-Cu alloys, it is generally observed that it is not possible to dissolve all the alloying elements in the Al-rich phase by liquid quenching [9,10]. It can thus be expected that in the gas-atomised powder only a limited fraction of the copper is dissolved in the Al-rich phase. This is supported by the presence of θ phase in gas-atomised ASCM powder [3], whereas this phase is absent in SQ ASCM [7].

The above suggests that the Al-rich phase of gas-atomised powder contains a higher fraction of silicon and a lower fraction of copper and magnesium as compared to the Al-rich phase of the SQ ASCM alloys. The increased silicon fraction is expected to result in precipitation of the Si phase during DSC heating. The main exothermic effect in the gas-atomised ASCM powder is observed between 430 and 510 K. This temperature range corresponds closely to the temperature ranges observed for silicon precipitation in hypereutectic rapidly solidified Al-Si alloys [9]. From this it is assumed that this exothermic effect is mainly caused by silicon precipitation. Using the enthalpy of silicon precipitation from the Al-rich phase, ΔH_{Si} (54 kJ/mole Si, see [9]), it is now possible to estimate the atomic silicon fraction in the Al-rich phase after gas atomisation from:

$x_{Si}=\Delta Q_{MP}/ (x_\alpha.\Delta H_{Si})$,

in which x_α is the fraction of Al-rich phase (α) in the gas-atomised powder (approximately equal to the fraction of Al atoms in the alloy, 0.78). Using this expression, a value of 0.014 is found for x_{Si}. This is indeed much larger than the maximal equilibrium solid solubility of Si in the Al-rich phase in ASCM alloys which equals about 0.004 [8].

The DSC scan of the gas-atomised ASCM powder shows a small endothermic effect just in advance of the main exothermic effect. Endothermic effects in this temperature range are indicative for

GP-zone dissolution (see section 3.3 and [7]). The GP-zone dissolution effect in the gas-atomised powder is much smaller than the GP-zone dissolution effect in SQ ASCM alloys (in the SQ ASCM alloys GP-zone formation mainly involves the formation of Al-Cu-Mg type GPB zones). This corroborates the above assumption that the atomic fractions of Mg and Cu atoms in the Al-rich phase of the ASCM powders are lower than in the Al-rich phase of the SQ ASCM0 alloy.

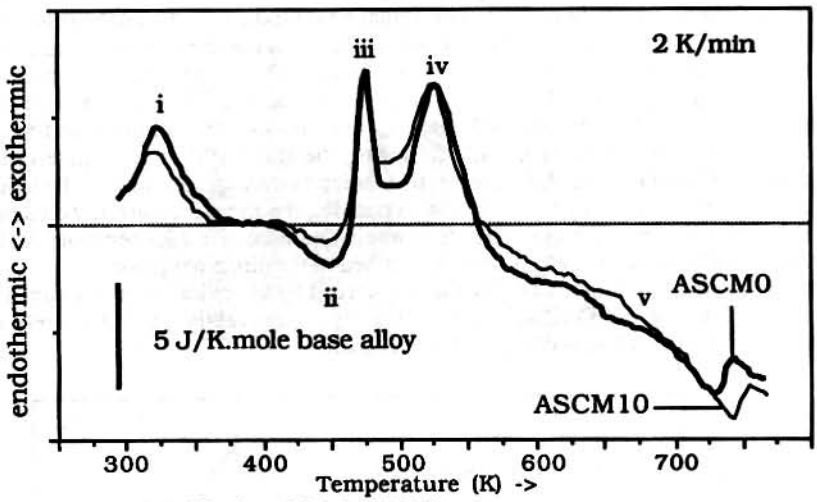

Fig. 6 : DSC scans of SQ ASCM0 and SQ ASCM10.

From about 590 K to the end temperature of the DSC scan, 773 K, the first DSC scan of the gas-atomised powder is dominated by a broad exothermic effect. As the Mg_2Si phase is unstable in the solid ASCM alloys, this phase must eventually transform into Q phase. As this is a thermally activated reaction from a stable to a metastable state, this transformation involves an exothermic reaction with a clearly defined peak temperature. Since no clear peak is observed in the first run on LQ ASCM0 beyond 590 K, the exothermic heat flow beyond 590 K is thought to be largely unaffected by this transformation. The temperature range of the broad exothermic effect in the DSC scan of gas-atomised powder is much broader, and located at much higher temperatures, than the ones usually encountered in the case of precipitation reactions. Indeed, no such effect is observed in DSC scans of SQ ASCM (see section 3.3). The second and the third scans of the gas-atomised powder do not show this exothermic effect. Instead they show only endothermic effects, which, over a large temperature range, resemble the corresponding parts of the first and second run of the AE ASCM0 alloy. These endothermic effects are caused by the dissolution of the Q, Si and θ phases (see section 4.2). Close to the end temperature of the DSC scan, also the second and the third DSC scans deviate from the scans of the AE ASCM0 specimen: beyond 750 K the endothermic heat flow seems to decrease in the powders. These effects, and the broad exothermic effect in the first run, are thought to be caused by oxide formation on the surface of the powders. This will be substantiated below.

During heating of gas-atomised Al-based alloys a series of reactions occur on the surface of the powders. These reactions involve the evolution of gases, and include [11]:

$$Al(OH)_3 \rightarrow AlOOH + H_2O \quad (5)$$

$$2\,AlOOH \rightarrow Al_2O_3 + H_2O \quad (6)$$

$$2/3\,Al + H_2O \rightarrow 1/3\,Al_2O_3 + H_2 \quad (7)$$

The water consumed during reaction 7 can either be provided by reactions 5 and/or 6, or H_2O molecules adsorbed by the oxide layer can be used. If sufficient oxygen is present also the direct oxidation reaction can occur:

$$4/3\,Al + O_2 \rightarrow 2/3\,Al_2O_3 \quad (8)$$

From these four reactions reaction 8 results in the largest enthalpy change (1.68 MJ per Al_2O_3 mole at 700 K, see Appendix). Because of their high specific surface area (0.17 m^2/g), surface reactions can

cause a significant heat evolution during DSC experiments on the gas-atomised ASCM powder (see Appendix). Since oxide layers on Al are always in the order of 10 to 100 nm, and since the gas-atomised powder already possesses a 40 nm thick oxide layer [3] it is assumed that the thickness of the oxide layer formed during the DSC run is of the order of 10 nm. The formation of a 10 nm thick oxide layer by reaction 8 produces about 3.1 kJ per mole powder. The formation an identical oxide layer by reaction 7 produces about 1.7 kJ per mole powder. The heats produced by reactions 5 and 6 are about one order of magnitude smaller. The actual heat production during heating of the powder inside the DSC is estimated from the area between the first and the third run in the temperature range where the effect occurs (590 to 773 K). This gives the value 1.6 kJ per mole powder, which agrees fairly well with the above presented estimates for the formation of a 10 nm oxide layer. It is however not possible to distinguish between the two oxide-formation modes (reactions 7 and 8). The mass of the gas-atomised powder increases by 0.17% during the three DSC runs. Since only the direct oxidation (reaction 8) results in a mass increase, this indicates that, at least, part of the oxide formation during the DSC scan is caused by this reaction. Assuming the mass increase to be caused by direct oxidation, a 0.17% mass increase corresponds to a released heat of 1.7 kJ per mole ASCM powder. Thus, the released heat measured can entirely be ascribed to the direct oxidation.

Apparently a significant amount of O_2 is either adsorbed by the oxide layer or trapped between the powder particles forming the DSC specimen. This O_2 is apparently not completely removed by flushing with argon before the start of the DSC experiment.

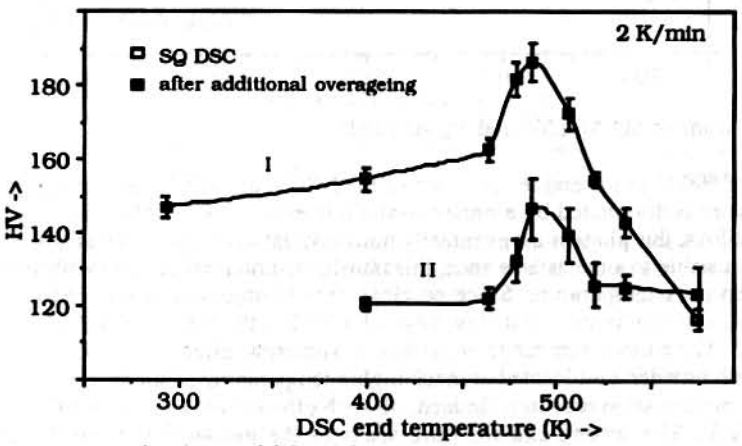

Fig. 7 : Room-temperature hardness of SQ DSC ASCM0 specimens as a function of the DSC end temperature (curve I). Also the hardness of these specimens after an additional overageing treatment (4 days at 473 K) is given as a function of the DSC end temperature (curve II).

4.2 MELTING AND DISSOLUTION REACTIONS IN AE ASCM

The peak temperatures of the exothermic and the endothermic effects appeared to be insensitive to variations of the heating rate. Therefore these endothermic effects are thought to be related to processes that are, to a large extent, equilibrium processes. As Al_2O_3 particles are supposed to be inert, this implies that these effects are insensitive to addition of Al_2O_3 particles, as has been observed.

From phase diagrams of the Al-Cu-Mg-Si system [8,12], it can be deduced that in the ASCM alloy no melting reaction occurs below 780 K. It is well established in literature that endothermic effects occurring between about 350 K and the melting of Al-Cu-Mg, Al-Cu-Si and Al-Cu-Mg-Si type alloys, are caused by the dissolution of alloying elements in the Al-rich phase (see for instance [7]). Accordingly, the endothermic effects in Fig. 4 are ascribed to dissolution of Cu, Mg and Si atoms in the Al-rich phase (since the maximum solid solubility of Fe in the Al phase is lower than 0.01 at% [8], the dissolution of Fe is neglected). From phase diagrams of the Al-Cu-Mg-Si system [8,12], it can be deduced that for the ASCM alloy the dissolution of the θ phase will be completed between 733 and

775 K. This is confirmed by high-temperature X-ray diffraction (see [7]), during which θ-phase lines disappear at 745±10 K. Thus it is concluded that the endothermic effect between 610 and 740 K mainly concerns θ-phase dissolution. As the Si phase and the Q phase are present on the whole temperature range of the high-temperature X-ray diffraction experiment, the remaining part of the dissolution effect is caused by continuing dissolution of the Q and Si phases.

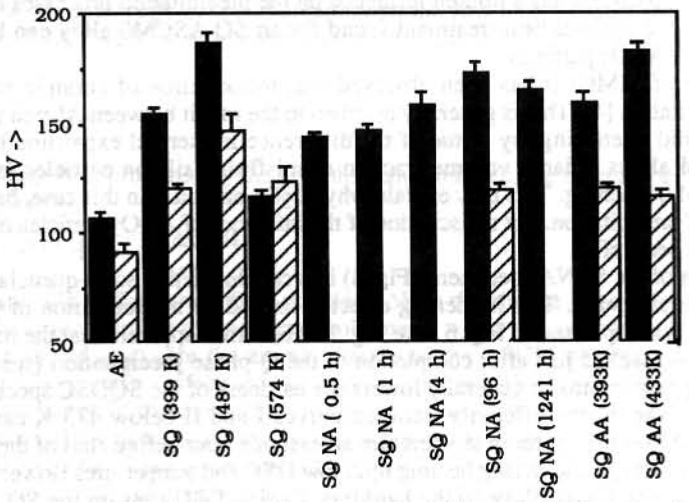

Fig. 8 : Room-temperature hardness of various heat treated samples (black bars). For some of the specimens also the hardness after an additional overageing treatment (4 days at 473 K) is given (grey bars).

An AE ASCM10 specimen heated twice to 870 K shows severe clustering of Al_2O_3 particles (see Fig. 3), which indicates that a large part of the alloy (including the Al-rich phase) had been melted. The endothermic effects in Fig. 5 are much larger than those in Fig. 4. Since melting reactions generally involve much larger enthalpy changes as solid state reactions do, and since in Al-rich Al-Cu-Mg-Si alloys the first stage of melting can occur starting from about 780 K [8], the endothermic effects occurring in Fig. 5 are ascribed to melting reactions. From Fig. 5 it is concluded that the melting of the base alloy of ASCM10 is devided into four stages A, B, C and D (the melting point of Al_2O_3 particles, about 2300 K, lies far beyond the DSC temperature range). Considering the solidification reactions denoted by the liquidus surface of the Al-Cu-Mg-Si system (see section 4.1), reaction D is clearly related to the melting of Si phase and Mg_2Si phase. Since effect C represents by far the largest endothermic heat content, this effect must be related to the melting of the (majority) Al-rich phase by the inverse of reaction 4. From the above it is is clear that the remaining reactions (reactions A and B) must be linked to the melting of the Q and Al_7Cu_2Fe phases. From literature [8] it is known that in Al-Cu-Mg-Si alloys various reactions involving the melting of the Q phase can occur in the temperature range 780 to 802 K. It is also known (from [8]) that in Al-Cu-Fe-Mg and in Al-Cu-Fe-Si alloys eutectic melting of the Al_7Cu_2Fe phase occurs at 778 and 793 K, respectively (data on the Al-Cu-Fe-Mg-Si system are unknown until now). So, the known temperature ranges of the Q and Al_7Cu_2Fe-phase melting reactions, while confirming that these two reactions are linked with the observed reactions A and B, give no clear indication which of the two phases melts first. However, in Fig. 5, reaction B is absent during the third run. This is interpreted as follows. During the second run, at the end of which the specimen is almost entirely melted, the melt reacts with the aluminum pan. This decreases the concentrations of Cu, Mg, Fe, and Si atoms in the alloy. From the Al-Cu-Mg-Si phase diagram at 775 K [8] follows that a decrease of the percentage of Mg in these alloys can result in dissolution of the Q phase in the Al-rich phase below 775 K. Then, melting of the Q phase will not occur. So, from the absence of the effect B in the third run of Fig. 5, it is concluded that effect B is

most likely caused by the melting of the Q phase. Then, effect A has to be caused by melting of the Al_7Cu_2Fe phase.

4.3. PRECIPITATION IN SQ ASCM

The hardness of an alloy is closely related to its microstructure. From Fig. 6 follows, that the presence of Al_2O_3 particles has a limited influence on the precipitation processes in SQ ASCM (see also [7]). Hence, the optimal heat treatment found for an SQ ASCM0 alloy can be applied for SQ ASCM alloys with Al_2O_3 particles.

For a number of MMCs it has been observed that introduction of ceramic particles alters the kinetics of precipitation [4]. This is generally ascribed to the misfit between Al-rich phase and ceramic particles after solid quenching, by virtue of the difference in thermal expansion [4]. In the Al-rich phases of ASCM alloys, a large volume fraction of misfitting silicon particles (about 22 vol%) is present after solid quenching. This may explain why Al_2O_3 particles, in this case, have little influence on the kinetics of precipitation. For a discussion of the influence of Al_2O_3 particles on the precipitation in ASCM alloys, see Ref. 7.

From hardness of the SQNA specimens (Fig. 8) it is concluded that solid-quenched ASCM0 can be hardened by natural ageing. This hardening effect is caused by the formation of GPB (Al-Cu-Mg) zones [13]. From a comparison of Fig. 6 with Fig. 7, it becomes apparent that the maximum hardness for SQ ASCM0 is reached just after completion of the Q-phase precipitation (see section 3.3). The additional overageing treatment generally lowers the hardness of the SQDSC specimens (see curve I and II in Fig. 7). The initial difference between curves I and II below 473 K can be explained as follows. SQ ASCM0 is kept at room temperature at least one hour before start of the DSC run. During room-temperature storage and during heating upto low DSC end tempertures (lower than 400 K) GPB zones are formed, which contribute to the hardness. During DSC runs on the SQ ASCM alloys the GPB zones start to dissolve from about 400 K, but dissolution is not completed before 473 K (see Fig. 6). The additional overageing treatment is sufficient to allow the dissolution of the GPB zones, leading to a marked drop in hardness. Besides the dissolution of GPB zones, also the annealing out of dislocations (formed during quenching, see [7]) can cause softening of the quenched specimens.

From the foregoing discussion it becomes apparent that two reactions contribute to the hardening of SQDSC ASCM0: i. GPB-zone formation and ii. Q-phase precipitation. Also the hardness changes of the specimens presented in Fig. 8 are interpreted in terms of these two hardening mechanisms.

Natural ageing results in GPB-zone formation. Thus increasing the time of natural ageing results in an increasing hardness (see Fig. 8). The slight decrease in hardness after long-time natural ageing may be related to relaxation of elastic tensions originally present after solid quenching [14]. As Q-phase formation occurs at temperatures around 480 K, the hardness increase observed on artificial ageing at 393 and 433 K is probably also due to GPB-zone formation. In the SQAA(433 K) specimen also θ' and Al-Cu type GP-zones might contribute to the hardness [13,15]. Since both GP zones and θ' are unstable, this explains why after additional overageing the hardness of the SQ AA specimens is reduced to about the same value as is observed for the SQNA specimen and the SQDSC specimens with DSC end temperatures lower than 473 K after the additional overageing treatment.

5. CONCLUSIONS

- The Q and Al_7Cu_2Fe phases, which are not (completely) dissolvable in the Al-rich phase, start melting from 780 K. Hence, the optimal solution treatment temperature is just below 780 K. The Al-rich phase of the ASCM alloys melts between 810 and 840 K.
- The hardness of the extruded ASCM alloy can be increased by about 75% by heat treatments which produce either GPB zones or Q-phase precipitates (ageing temperatures 433 to 500 K).
- For high-temperature applications, only ageing treatments at temperatures around 480 K, giving rise to the formation of the Q phase, are usefull. These ageing treatments can increase the room-temperature hardness of the ASCM0 alloy by about 60% (as compared to the as extruded alloy).
- The presence of Al_2O_3 particles in the ASCM alloy has little influence on the precipitation after solid quenching.

ACKNOWLEDGEMENTS

The authors are indebted to Mr. J. F. van Lent for performing the Guinier camera experiment and to Dr. J. Duszczyk for providing the alloys. Stimulating discussions with Professor B. M. Korevaar, Dr. J. Duszczyk and Dr. W. H. Kool are gratefully acknowledged.

The financial support of the Foundation for Fundamental Research of Matter and for Technological Sciences (FOM/STW) is gratefully acknowledged. Also the financial support from the European Community program ERASMUS for one of the authors (V. J.) is gratefully acknowledged.

APPENDIX

The exothermic heat effect produced by the growth of aluminium oxide layers of average thickness, d, on powders, is given by:

$$\Delta Q_{ox} = A_S \cdot d \cdot \Delta H \cdot \rho_{ox} \cdot \frac{M_{ASCM}}{M_{Al_2O_3}}$$

in which A_S is the specific surface area of the powders, ΔH is the change in enthalpy of the reacting substances due to the oxide forming reaction, per mole oxide, ρ_{ox} is the average density of the oxide layer, and M_{ASCM} and $M_{Al_2O_3}$ are the atomic masses of the ASCM powder (27.7 g/mole) and Al_2O_3 (102 g/mole). The specific surface area of the gas-atomised ASCM powders equals 0.17 m^2/g [3]. For the enthalpy change of the oxide forming reactions, ΔH, the value of ΔH at 700 K is used (the small variations of ΔH with temperature, about 1% per 100K at 700K [16], are neglected). Then ΔH is given by 0.95 and 1.68 kJ per mole Al_2O_3 for reactions 7 and 8, respectively [16]. The ΔH of reaction 6 is about one order of magnitude smaller [11]. The density of fully dense α-Al_2O_3 (corrundum) equals 3.98 g/cm^3. This value will be used as an estimate for ρ_{ox}.

REFERENCES

1 D. Bialo, J. Duszczyk, A.W.J. de Gee, G.J.J. van Heijningen and B.M. Korevaar, Wear, vol. 141, 1991, pp. 291-309.
2 D. Bialo, T.L.J. de Haan and J. Duszczyk, Internal Technological Report, Oct. 1989, Delft University of Technology.
3 J.L. Estrada and J. Duszczyk, J. of Mater. Sci., vol. 25, 1990, pp. 886-904.
4 J. M. Papazian, Metall. Trans. A, vol. 19A, 1988, pp. 2945-2953.
5 J.H. ter Haar and J. Duszczyk, Mater. Sci. and Eng., vol. A135, 1991, pp. 65-72.
6 D.S.Phillips, T.E. Mitchell and A.H. Heuer, Phil. Mag. A, vol.42, 1980, pp. 417-432.
7 M.J. Starink, V. Jooris and P. van Mourik, Proc. Conf. on Mater. Sci.: MMCs-Processing, Microstructure and Properties, Roskilde, Denmark, 2-6 september 1991, submitted for publication.
8 L.F. Mondolfo: Aluminium Alloys, Butterworth & Co Ltd, London, 1976.
9 M. van Rooijen and E.J. Mittemeijer, Metall. Trans. A, vol. 20, 1989, pp. 1207-1214.
10 Q. Li, E. Johnson, A. Johansen and L. Sarholt-Kristensen, Proc. Int. Conf. on Advanced Al and Mg Alloys, Amsterdam, The Netherlands, 20-22 june 1990, T. Khan and G. Effenberg, eds., pp. 349-356.
11 J.L. Estrada, J. Duszczyk and B.M. Korevaar, J. of Mater. Sci., vol. 26, 1991, pp. 1631-1634.
12 H.J. Axon, J. of the Institute of Metals, vol. 83, 1955, pp. 490-492.
13 W. Bonfield and P.K. Datta, J. of Mater. Sci. Lett., vol. 11, 1977, pp. 1050-1052.
14 J.G.M. van Berkum, R. Delhez, Th. H. de Keijser, E.J. Mittemeijer and P. van Mourik, submitted to Sripta Metall.
15 A.K. Gupta, M.C. Chaturvedi and A.K. Jena, Mater. Sci. and Techn., vol. 5, 1989, pp. 52-55.
16 I. Bahrin: Thermochemical Data of Pure Substances, VCH Verlagsgesellschaft, Weinheim, BRD, 1989.